LIMNOLOGY
and
OCEANOGRAPHY

ASLO

Limnol. Oceanogr. 00, 2019, 1–17

doi: 10.1002/lno.11162

Internal waves influence the thermal and nutrient environment on a shallow coral reef

Emma C. Reid,[1*] **Thomas M. DeCarlo**,[2,3] **Anne L. Cohen**,[2] **George T. F. Wong**,[4,5] **Steven J. Lentz**,[2] **Aryan Safaie**,[1] **Austin Hall**,[6,7] **Kristen A. Davis**[1]

[1]Department of Civil & Environmental Engineering, University of California, Irvine, California
[2]Department of Geology and Geophysics, Woods Hole Oceanographic Institution, Falmouth, Massachusetts
[3]Australian Research Council Centre of Excellence for Coral Reef Studies, University of Western Australia, Crawley, Western Australia, Australia
[4]Research Center for Environmental Changes, Academia Sinica, Taipei, Taiwan
[5]Department of Ocean, Earth and Atmospheric Sciences, Old Dominion University, Norfolk, Virginia
[6]Department of Biological and Ecological Engineering, Oregon State University, Corvallis, Oregon
[7]Division of Integrated Regional Water Management, California Department of Water Resources, Sacramento, California

Abstract

Internal waves can influence water properties in coastal ecosystems through the shoreward transport and mixing of subthermocline water into the nearshore region. In June 2014, a field experiment was conducted at Dongsha Atoll in the northern South China Sea to study the impact of internal waves on a coral reef. Instrumentation included a distributed temperature sensing system, which resolved spatially and temporally continuous temperature measurements over a 4-km cross-reef section from the lagoon to 50-m depth on the fore reef. Our observations show that during summer, internal waves shoaling on the shallow atoll regularly transport cold, nutrient-rich water shoreward, altering near-surface water properties on the fore reef. This water is transported shoreward of the reef crest by tides, breaking surface waves and wind-driven flow, where it significantly alters the water temperature and nutrient concentrations on the reef flat. We find that without internal wave forcing on the fore reef, temperatures on the reef flat could be up to 2.0°C ± 0.2°C warmer. Additionally, we estimate a change in degree heating weeks of 0.7°C-weeks warmer without internal waves, which significantly increases the probability of a more severe bleaching event occurring at Dongsha Atoll. Furthermore, using nutrient samples collected on the fore reef during the study, we estimated that instantaneous onshore nitrate flux is about four-fold higher with internal waves than without internal waves. This work highlights the importance of internal waves as a physical mechanism shaping the nearshore environment, and likely supporting resilience of the reef.

Internal waves are a persistent feature throughout the world's oceans and can have significant physical and biological impacts on marine ecosystems (Garrett and Munk 1979; Woodson 2018). Much attention in the literature has been given to internal waves on the middle and outer continental shelves (Nash et al. 2012; Alford et al. 2015) and increasingly we are learning more about their influence in the inner shelf and nearshore environment (Walter et al. 2012; Sinnett and Feddersen 2014; Walter et al. 2014). Shoaling internal waves can transport cold and nutrient-rich water into shallow coastal regions and have been observed to modify water properties and influence the metabolism of benthic communities in coastal ecosystems such as kelp forests and coral reefs (Wolanski and Pickard 1983; Zimmerman and Kremer 1984; Wolanski and Delesalle 1995; Leichter et al. 1996; McPhee-Shaw et al. 2007; Noble et al. 2009; Hofmann et al. 2011; Lucas et al. 2011; Green et al. 2018).

The accelerating degradation of coral reefs over the past 50 yrs, in part, due to rising ocean temperatures, has led to predictions of a global-scale collapse in reefs within the next few decades (Hoegh-Guldberg et al. 2007; Donner 2009; Van Hooidonk et al. 2016). However, variation in the physiological responses of individual coral colonies and reefs to environmental stresses suggests critical differences in corals' resilience and/or environmental conditions over small spatial and temporal scales (Riegl and Piller 2003; Pandolfi et al. 2011; van

*Correspondence: reide@uci.edu; davis@uci.edu

Additional Supporting Information may be found in the online version of this article.

Woesik et al. 2011; van Woesik et al. 2012). For example, water temperatures and thermal tolerance can vary substantially across an individual reef (e.g., Pineda et al. 2013; Palumbi et al. 2014; Safaie et al. 2018) and some coral communities thrive in naturally acidified waters (Shamberger et al. 2014; Barkley et al. 2015). Thus, coral organisms with greater resilience and adaptive capacity may persist under future climate change (Pandolfi et al. 2011; Spalding and Brown 2015). Identifying these resilient corals and prioritizing their protection may be the best strategy for long-term conservation of coral ecosystems (Barshis et al. 2013). Although the factors which confer resilience to coral bleaching are not fully understood, emerging evidence suggests that corals living in areas with naturally variable thermal environments may have higher temperature tolerance (McClanahan et al. 2005; Safaie et al. 2018). Thus, there are strong conservation incentives for investigating the drivers of high-frequency (diurnal or shorter timescales) temperature variability on reefs, including air–sea heat fluxes (e.g., Davis et al. 2011) and internal waves (e.g., Wolanski and Delesalle 1995; Leichter et al. 1996; DeCarlo et al. 2015).

Dongsha Atoll, a coral reef and Taiwanese National Park in the northern South China Sea (SCS), is directly in the path of some of the world's largest internal solitary waves (with amplitudes of 100–150 m) generated by tidal currents in the Luzon Strait (Hsu and Liu 2000; Alford et al. 2015). These internal waves shoal and form bottom-propagating internal bores—internal waves of elevation, where the strongest currents and temperature fronts are near the bed—and boluses on the shallow topography of the reef system and the surrounding shelf, injecting cold, nutrient-rich water onto the fore reef (Wang et al. 2007; Fu et al. 2012; Alford et al. 2015; DeCarlo et al. 2015). We examine benthic thermal environments using a distributed temperature sensing (DTS) system, which resolves spatially continuous temperature measurements along a fiber optic cable. A 4-km cable was deployed from the east fore reef to the lagoon (Fig. 1). We show that internal waves modify the surface water properties on the fore reef and that this water is transported onshore by tides, surface waves, and wind. Using the DTS measurements, we then quantify the effect of internal waves on the temperature and nutrient environment on the shallow reef flat.

Methods

Site description

Dongsha Atoll is 28 km in diameter and has an area of approximately 600 km^2 (Dai 2004). The east reef flat, which is the focus of this article (Fig. 1b), is roughly 3 km wide and ranges from 0.6 to 3.5 m in depth. The tidal range on the reef flat is approximately 0.9 m. The fore reef has a gradual 4% slope down to 25 m depth, beyond which it steepens to 15%. A survey of the benthic composition of the reef flat shows the region is dominated by fleshy algae, sea grass, and live coral (DeCarlo et al. 2017*b*). The reef slope has a spur and groove formation, which is dominated by soft corals.

General ocean circulation in the northern SCS during the summer is controlled by monsoon winds (Hu et al. 2000). Winds from the southwest drive surface currents generally to the northeast (Morton and Blackmore 2001). A seasonally occurring cyclonic eddy, known as the Dongsha cyclonic eddy (DCE), typically appears south or southwest of Dongsha Atoll during the late spring and summer, and propagates to the southwest (Chow et al. 2008).

Internal waves generated in the Luzon Strait travel westward as solitary waves of depression, and transform into waves of elevation as they shoal on the shallowing shelf topography in water depths < 200 m (Fu et al. 2012). The travel time between generation in the Luzon Strait and Dongsha Atoll is approximately 2 d (Ramp et al. 2010). When the waves reach depths < 30 m, they become highly nonlinear internal bores and boluses and transport cold, subthermocline water into the nearshore region (Leichter et al. 2003; Wang et al. 2007; Moore et al. 2016). Below, we will consider our study site as two adjacent dynamic systems: (1) the region offshore of the reef crest where shoaling internal waves are dominating cross-shore flows and influencing near-surface water properties, and (2) the reef flat region onshore of the reef crest where tides, wind, and surface waves dominate the circulation, and bring offshore water onto the reef. Here, we assume that internal waves do not play an important role in driving flow on the reef flat but instead are important in setting the water properties of the offshore boundary condition.

Experiment

The observations presented here are part of a larger study of coral ecology, reef-scale circulation, and internal wave dynamics at Dongsha Atoll (DeCarlo et al. 2017*b*). In this study, we will focus on measurements of currents, water temperature, nitrate concentrations, and meteorological conditions on the reef slope and flat on the east side of the atoll (Fig. 1b), collected from 04 to 11 June 2014. This study took place during the summer monsoon season in the SCS and was interrupted by Tropical Storm Hagibis on 12 June, when the DTS instrument lost power.

Two 2-MHz Nortek AquaDopp Profilers were placed on the reef flat at E3 and E5 (Fig. 1b) to measure currents and pressure at 4-min intervals. The depth at E3 and E5 were on average 0.6 and 1.9 m, respectively. An upward-looking Acoustic Wave and Current Profiler (Nortek AS) was deployed at 18.1 m depth at E1 and recorded current measurements at 1-min intervals and measured surface wave statistics in 20-min bursts every 3 h.

Water samples were collected using GO-FLO bottles mounted onto a rosette sampling assembly (General Oceanic) aboard the Taiwanese vessel Ocean Researcher 3 on 04–05 June 2014 at E1, approximately 450 m from the reef crest, at 2, 5, and 10 m depths every 3 h and analyzed for nitrate concentrations.

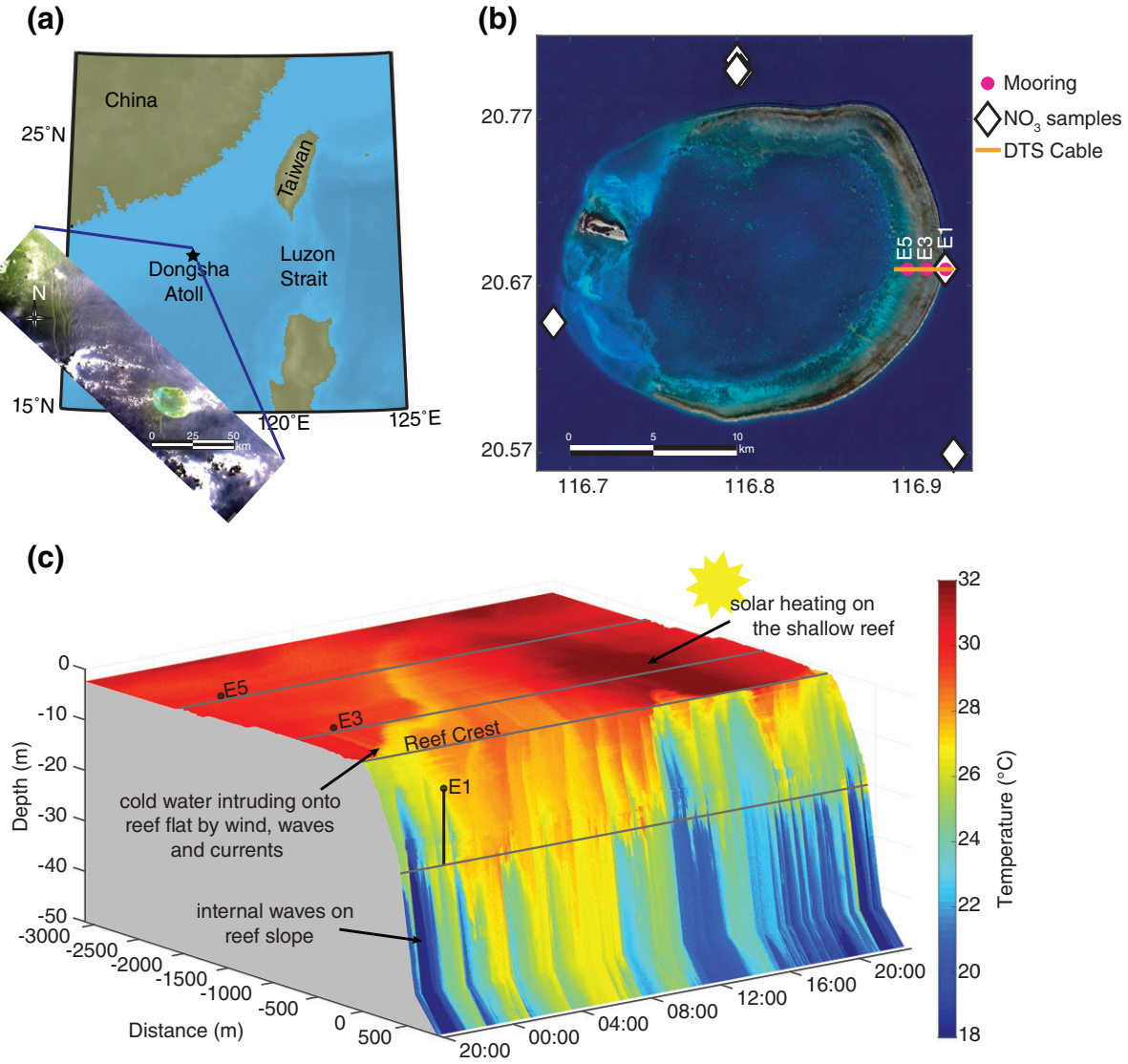

Fig. 1. Oceanographic setting of the Dongsha Atoll. Panel **a** The location of Dongsha Atoll within the northern SCS; and Panel **b** is a satellite view of the atoll with locations of the DTS cable as an orange line across the east reef flat and slope and Moorings E1, E3, and E5 in pink. Nitrate/temperature sample locations are shown in white diamonds. Two nitrate/temperature sample locations not shown are located at [117.56, 20.760] and [117.63, 20.79]. Panel **c** is a three-dimensional cross section of the reef slope and flat with temperature data from the DTS and includes the locations of instrumentation on the reef at E1, E3, and E5.

Additional discrete water samples for the determination of nitrate were collected on October 2012 at seven locations in the waters surrounding Dongsha (Fig. 1b), aboard Ocean Researcher 1. The samples were quick-frozen with liquid nitrogen onboard ship and returned to a shore-based laboratory for the determination of nitrate with a precision of about $\pm$ 0.2 μmol L^{-1} (Wong et al. 2015*a*,*b*; Wong et al. 2017).

The meteorological data used in this study were measured from a ēKo Pro Series meteorological station on top of a platform located in a sand patch on the reef flat at E5 (Fig. 1b). The station carries sensor suites for measuring wind speed and direction, air temperature, relative humidity, barometric pressure, incoming shortwave radiation, and precipitation, which allow for estimates of the air–sea exchange of heat.

Additionally, Level-2 (11 μm) swath sea surface temperature (SST) from the Moderate Resolution Imaging Spectroradiometer (MODIS) instrument aboard the Aqua and Terra satellites, with native spatial resolution of $\sim 1 \times 1$ km^2, was used for the heat budget analysis. These data were obtained from the NASA Ocean Color Web (http://oceancolor.gsfc.nasa.gov/, accessed 02 July 2018) and have been observed to compare well to in situ observations at Dongsha Atoll (Pan et al. 2017).

A 19-yr (1992–2010) high-resolution (0.1°× 0.1°) ocean reanalysis dataset (called REDOS) of the upper ocean in the SCS from Zeng et al. (2014) was used to evaluate the general ocean circulation patterns during summer months.

Tidal velocities in the Luzon Strait were estimated using the Oregon State Tidal Inversion Software (Egbert and Erofeeva 2002) and the TMD toolbox (Padman and Erofeeva 2004).

DTS setup and calibration

Raman spectra fiber-optic DTS technology was deployed across the Dongsha east reef slope and reef flat to measure temperature at the bed over a 4-km distance. A Sentinel Oryx DTS interrogator collected continuous independent temperature measurements every 2 m along a Kaiphone (flexible white, 6 mm, steel-reinforced) fiber optic cable at a sampling frequency of one temperature trace per minute, providing a spatially continuous perspective of near-bed temperature in a cross-shelf section. In DTS, a coherent pulse of light is sent down the cable, and continuous measurements of Raman backscattered light spectra allows for determination of the temperature at each point in the cable (Tyler et al. 2009; Hausner et al. 2011). DTS technology has been used in various environmental monitoring programs in the past, providing high spatial (< 1 m) resolution temperature measurements at scales of meters to kilometers (Selker et al. 2006; Tyler et al. 2009; Hausner et al. 2011; Suárez et al. 2011; Vercauteren et al. 2011; Van Emmerik et al. 2013; Kobs et al. 2014; Zeeman et al. 2014).

The fiber optic cable was deployed in the cross-shelf direction on the east reef flat, starting near the lagoon and going east across the reef flat and down the reef slope to a depth of approximately 50 m (Fig. 1c). The Oryx was mounted on a platform setup at E5 (Fig. 1c), from which a 1-km section of fiber-optic cable was deployed toward the lagoon and a 3-km cable was deployed in the offshore direction. Calibration of the raw DTS data was performed following Hausner et al. (2011). The two cables were deployed in simple single-ended configurations on the reef, with 12 accurate temperature sensors (Seabird Electronics SBE-56s, ± 0.002°C) placed for calibration (6 sensors) and validation (6 sensors). The calibration sections were held at a relatively constant temperature throughout the deployment; however, due to the dynamic nature of internal waves, obtaining a uniform, steady temperature for the calibration reference point offshore was difficult. The eastern terminal end coil saw dramatic fluctuations in temperature when internal waves arrived at the reef slope. For this reason, a 30-min low-pass filter (LPF) was applied to the calibration coefficients.

The average root mean square error (RMSE) and bias calculated for the validation loggers was 0.20°C ± 0.02°C and 0.07°C ± 0.01°C, respectively. When the RMSE value for the validation logger was over a threshold of 0.35°C, the calibration coefficients were removed and linearly interpolated, and temperature was recalculated, along with RMSE and bias of the recalibration.

Estimating tide-, wave-, and wind-driven flow

An analysis of the currents on the Dongsha reef flat at E3 and E5 and on the reef slope at E1 was performed to determine the physical processes which govern flow in these regions. On the reef flat, a simple model of tide-, wind-, and surface wave-driven flow was created.

Barotropic tidal currents on the reef flat are estimated using the depth averaged currents and a unified tidal analysis and prediction method (Codiga 2011). Wave- and wind-driven flow on the reef flat is estimated following Lentz et al. (2016):

$$u = \mathrm{sgn}\left(-\frac{S_{xx}}{\Delta x} + \tau^{sx}\right)\sqrt{\frac{-\frac{S_{xx}}{\Delta x} + \tau^{sx}}{\rho C_{\mathrm{da}}}} \tag{1}$$

where u is the cross-shore velocity, positive toward the east, S_{xx} is the cross-reef component of the wave-radiation stress tensor, Δx is the width of the region of wave breaking and reef flat, which is taken as 3000 m, τ^{sx} is the wind stress, and ρ is the density of seawater. C_{da} is the bulk drag coefficient, which is estimated as follows:

$$C_{\mathrm{da}} = \kappa^2\left\{\log\left(\frac{h}{z_0}\right) + (\Pi - 1)\right\}^{-2} \tag{2}$$

where $\kappa = 0.4$ is the von Karman constant, h is the time-variable water depth, $z_0 = 3.2$ cm is the hydrodynamic roughness estimated for our site in a previous study (Lentz et al. 2017), and Π is Cole's wake strength, which is taken as 0.2 (Lentz et al. 2016).

The wave-radiation stress tensor, S_{xx} is estimated as follows:

$$S_{xx} = \frac{\rho g {H_s}^2}{16}\left\{\left(\cos^2(\theta_w) + 1\right)\frac{c_g}{c} - \frac{1}{2}\right\} \tag{3}$$

where $g = 9.81$ ms^{-2} is gravitational acceleration, H_s is significant wave height measured at E1, θ_w is wave direction, c_g is group velocity, and c is phase velocity (Lentz et al. 2016).

Heat budget

A heat budget analysis was performed on the reef flat (1) to determine the physical processes that control temperature on the reef flat at Dongsha and (2) to predict water temperature on the reef flat without the influence of internal wave-induced cooling of the fore reef waters. A simple heat budget was estimated following Davis et al. (2011):

$$\frac{\partial \bar{T}}{\partial t} + \overline{u_i}\frac{\partial \bar{T}}{\partial x_i} = -\frac{\partial}{\partial x_i}\overline{u_i' T'} \tag{4}$$

where, the summative convention with the index i = 1–3 and a right-handed coordinate system is adopted with the principle axes defined by x_i, x is the distance across the reef, positive to the east, y is the distance along the reef, positive to the north,

and z is positive upward, u_i represents the corresponding velocity components, u, v, and w, and T is water temperature. Overbars denote time-averaged quantities (in this case, over 10-min), and primed values are the fluctuating components ($u = \bar{u} + u'; T = \bar{T} + T'$). The heat budget is focused on the cross-shore dimension only, because the alongshore flow, v, and vertical velocities, w, are an order of magnitude less than cross-shore flow, u. The temperature, T, is assumed to be well mixed in the vertical on the shallow reef flat.

Temporal sampling frequency was not sufficient for measuring turbulent transport of heat. Our results suggest that this term as well as heat flux through the reef bed are likely small, given the approximate balance between advective and atmospheric heat flux; see similar results in Davis et al. (2011).

When Eq. 4 is vertically integrated over the water column, and the equation is multiplied by the heat capacity per unit volume (ρc_p, assumed to be constant and equal to 4.1×10^6 W s m^{-3} °C^{-1}), we obtain an equation for the heat balance within a volume of water of unit length and width (Eq. 5; Davis et al. 2011). The left side of Eq. 5 represents the rate of change of heat storage within the volume, Q_T. The terms on the right side of the equation represent the advective heat flux, ΔF, and atmospheric/ocean heat flux, Q_N.

$$\rho c_p h \frac{\partial \langle \bar{T} \rangle}{\partial t} = -\rho c_p h \langle \bar{u} \rangle \frac{\partial \langle \bar{T} \rangle}{\partial x} + Q_N \tag{5}$$

$$OR \qquad Q_T = \Delta F + Q_N \tag{6}$$

where h represents the depth of the water, and u is the depth-averaged velocity in the cross-shore direction, and angled brackets denote depth averaged quantities. Velocity measurements in the top 1-m of the water column were missing due to acoustic reflection off the water surface. When the water depth at E3 was too shallow to estimate velocities, a linear relationship between transport at E5 and E3 was used to estimate velocities at E3. Various methods of estimating the velocities for the top of the water column were tested, including applying a log fit or an empirical orthogonal function fit to the data, or applying the available depth averaged currents to the entire water column, and all methods yielded very similar results. We used the latter method for this analysis, where the available depth averaged currents were applied over the entire water column, and a 1-h LPF was applied.

The net heat flux between the atmosphere and the ocean, Q_N, is calculated as follows:

$$Q_N = Q_E + Q_H + Q_S + Q_L \tag{7}$$

where the terms on the right-hand side of the equation represent latent, sensible, net shortwave, and net longwave heat flux, respectively. The net shortwave heat flux was measured at a meteorological station located on the platform at Sta. E5. The incoming shortwave radiation was corrected for an additional albedo (10%), to account for reflectance of the coral bed in shallow water (Maritorena et al. 1994). A modified version 2.5 Tropical Oceans Global Atmosphere Coupled Ocean–Atmosphere Response Experiment bulk algorithm (Fairall et al. 1996; Fairall et al. 2003) was used to compute the latent and sensible heat fluxes. The net longwave heat flux was calculated as follows (Rosenfeld et al. 1994):

$$Q_b = \epsilon\sigma(T + 273.16)^4(0.254 - 0.00495 R_H e_s) \tag{8}$$

$$e_s = 6.122 \times \exp\left(\frac{17.67 T_{air}}{T_{air} + 243.5}\right) \tag{9}$$

where Q_b is clear sky net longwave radiation, ϵ is the emissivity of the sea surface, taken as 0.97, σ is the Stefan–Boltzman constant, 5.6697×10^{-8} W m^{-2} K^{-4}, T is the SST in°C, R_H is the relative humidity measured by the meteorological station, e_s is the saturated vapor pressure, and T_{air} is the temperature of the air in°C. Finally, a linear cloud factor, (1–0.9°C), from Reed (1976), was applied to the net longwave radiation, where C is the cloud cover coefficient, taken as 0.59 for 20°N (Budyko 1974).

A heat budget focused on the reef flat near E3, where the spatial temperature gradient, $\partial\langle \bar{T} \rangle / \partial x$ in Eq. 5, is calculated over a 200-m distance, 100 m on either side of the current profiler, using the DTS temperature measurements. The 200-m spatial averaging is a compromise between resolving spatial gradients on the reef and measuring differences in temperature over this distance that exceed DTS instrument precision. A heat budget for the entire reef flat is estimated using 200-m averaged DTS temperature across the reef flat as an initial condition and a boundary condition of 1-h low-pass–filtered DTS temperature at the reef crest. Temperature on the reef flat was predicted from Eq. 5 using a forward differencing scheme for the time derivative and a central difference for the spatial gradient in temperature. Transport at E3 and E5 was calculated, using 1-h low-pass–filtered currents, and interpolated for the reef flat in between. The transport from E3 was used from the reef crest to E3, and the transport from E5 was used from E5 toward the lagoon. Atmospheric heat flux at each location on the reef was calculated using temperature from the time step before.

To compare the observed temperatures to the modeled heat budget temperatures, we use the Willmott Skill Score (WSS) (Willmott 1982), defined as:

$$WSS = 1 - \frac{\frac{1}{N}\sum_{i=1}^{i=N}(m_i - o_i)^2}{\frac{1}{N}\sum_{i=1}^{i=N}(|m_i - \bar{o}| + |o_i - \bar{o}|)^2} = 1 - \frac{MSE}{\frac{1}{N}\sum_{i=1}^{i=N}(|m_i - \bar{o}| + |o_i - \bar{o}|)^2} \tag{10}$$

where o_i is an observation, m_i is the corresponding model value, where there are N paired modeled/observed values, and MSE is the mean square error. A WSS value of 1 indicates perfect agreement between the observed and modeled values, and a value of 0 indicates no agreement.

Results

Circulation on the reef

Measurements from the meteorological station located on the reef flat showed that winds at the start of the study period, 04–06 June, were on average 6 m s^{-1}, and increased on 07–08 June, to an average of 8.5 m s^{-1} with gusts up to 22 m s^{-1}. From 09 to 11 June, winds gradually increased, with an average of 9 m s^{-1}. Incoming solar radiation showed diurnal heating on the reef, with a maximum of approximately 1000 W m^{-2}, except on 07–08 and 12 June, when maximum radiation was significantly lower, approximately 200 W m^{-2}, due to increased cloud cover (Fig. 2).

Currents on the reef flat (E3) during the study period in June 2014 were influenced by tides, surface waves, and wind stress and were estimated using tidal analysis and Eq. 1, where barotropic (surface) tides for 45%, surface waves for 24%, and wind stress for 26% of the variance in across-shore flows, with similar results at E5. As might be expected for a shallow reef flat, we did not find any significant relationship between currents on the reef flat and internal wave forcing on the fore reef slope offshore. However, offshore on the reef slope (E1, at 20 m isobath), the variance in across-shore flows near the reef bed (bottom 8 m) is dominated by bottom-propagating internal bores. Internal waves shoaling on the Dongsha fore reef slope have been observed in the form of nonlinear waves of elevation (Fu et al. 2012) and internal bores (K. A. Davis unpubl.). These waveforms can transport dense, cold fluid upslope toward the reef crest. We observed the shoaling of over 500 internal waves on the Dongsha fore reef in 11 d. The internal bores appear as a strong, cold temperature front in the DTS signal with apparent phase speeds of approximately 0.4 m s^{-1} and often transport cold water all the way to the surf zone. The focus of this study is what impact the internal-wave–modified water has on the reef flat community.

Spectral analysis of the across-shore component currents at E1 and E3 reveals a significant peak at the diurnal and semidiurnal frequency (Fig. 3a) on both the reef flat and reef slope. During a period of low winds (04–06 June), the depth averaged currents on the reef flat were primarily tidal from the ocean to the lagoon on flood and reversing on ebb. During a period of higher winds and waves, depth-averaged currents were directed primarily offshore on 07 and 08 June and onshore from 09 to 11 June. For this deployment, when significant wave height, H_s, was greater than 1.5 m, depth averaged currents on the reef were directed toward the lagoon and did not reverse with the tide.

Flushing time, T_f, was estimated for the reef flat at E3 and E5 as

$$T_f = \frac{V}{Q} \tag{11}$$

where V is the volume of water on the reef from the crest to 3-km toward the lagoon, and Q is the volumetric flow rate through the system (Monsen et al. 2002). Daily average flushing time during the study period ranged from 0.7 d to 2.1 $\pm$ 0.2 d, with the shorter flushing times occurring when wind and waves were stronger, forcing more flow across the reef.

Near-bed temperature across the reef

Although corals are typically thought to thrive in thermally stable environments (Glynn 1993; Goreau and Hayes 1994; Hoegh-Guldberg 1999), there is a large amount of temperature variability in both time and space on the reef flat (Fig. 2). The mean temperature on the reef flat from the lagoon to the reef crest is 29.4°C. The fore reef experiences a natural topographic slope break at about 25 m depth, with a shallow slope ($\sim$ 4%) from the reef crest to the 25-m isobath (approximately 425 m offshore of the reef crest) and a steep slope ($\sim$ 15%) from 25 to 50 m depth (the end of the cable). The mean temperatures on these two sections are 27.2°C and 23.6°C, respectively. The steep section of the fore reef experiences strong internal wave action and has a diurnal temperature range of 7.4–9.0°C, whereas corals on the shallow section of the fore reef experience a range of 4.5–8.2°C, because fewer internal waves propagate shoreward beyond the slope break.

In this time series, internal waves arriving at the atoll are seen on the fore reef slope as pulses of cold water accompanied by temperature decreases of approximately 4–8°C in less than 1 min. Typically, there are more frequent internal waves, with larger (6–8°C) temperature decreases evident near the spring tides (new moon on 29 May, and full moon on 13 June), and there are fewer internal waves, with smaller (2–4°C) temperature decreases arriving during the neap tide. The diurnal timescale variability of near-bed temperature on the fore reef does not appear to be controlled by atmospheric heating and cooling (Fig. 3b), unlike the reef flat, discussed below.

Water temperature on the reef flat exhibits much smaller diurnal temperature ranges than water on the internal wave-exposed fore reef slope. During the 8-d study period, corals on the reef flat (near E3) experienced diurnal temperature ranges of 1.3–5.8°C, primarily due to solar heating cycles. For example, in Fig. 2a–h, the reef flat (between –3000 and 0 m) experiences maximum temperatures (red patches) in the afternoon and this heating is modulated by the intensity of solar insolation (purple arrows on the right-hand side of Fig. 2 and also Fig. 3b). On 07–08 June when cloudy conditions caused reduced atmospheric heating, there was reduced heating on the reef flat (Fig. 2d,e) and the diurnal temperature range was 1.4°C, on average, while during days with clearer skies and increased solar forcing, daily temperature ranges averaged 4.9°C. When cumulative atmospheric heat flux was –85 W m^{-2} (due to clouds) on 07 June, the temperature range on the reef flat was 1.3°C. Whereas, on 06 June, when cumulative atmospheric heat flux was 94 W m^{-2} and circulation on the reef flat was similar, the temperature range on the reef flat was 5.8°C. The relationship between atmospheric heating and daily temperature range of the near-bed waters was much stronger in shallow reef flat waters

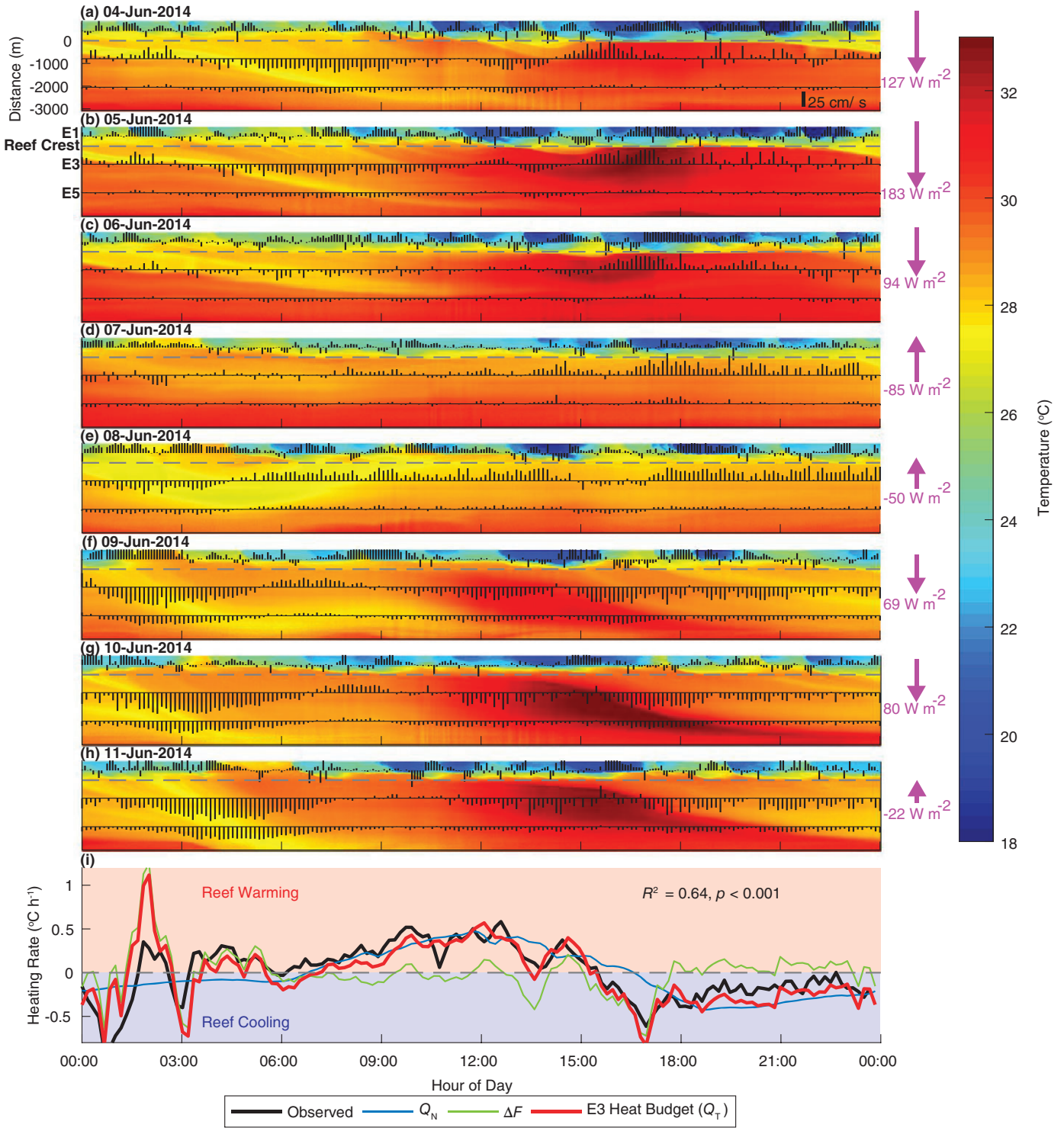

Fig. 2. DTS temperature data and the heat budget. Panels **a** to **h** show DTS temperature measurements for the 8-d period between 04 June 2014 and 11 June 2014. Across shore currents are shown at E1, E3, and E5 in black quivers, with quivers pointing down indicating onshore flow (to the west), and quivers pointing up indicating offshore flow (to the east). Cumulative net atmospheric heat flux for each day is shown with the magenta arrow indicating net heating (down) or cooling (up). The reef crest is indicated by thick dashed line at distance = 0 m. Panel **i** shows the daily composite heat budget at E3 for the study period. The black line is the observed heat flux, the blue line is the atmospheric heat flux, the green line is the advective heat flux, and the red line is the predicted net heat flux at E3.

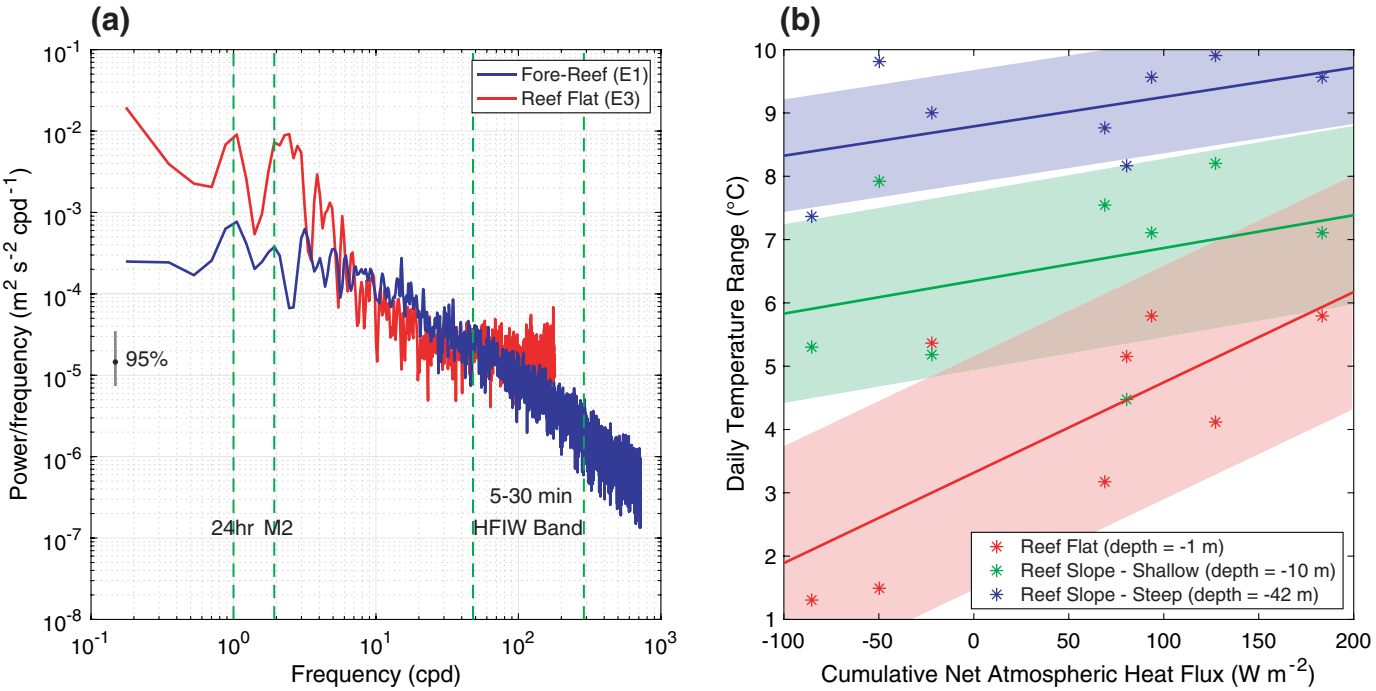

Fig. 3. DTS daily temperature range and power spectra of currents. Panel **a** shows the power spectra of currents on the reef flat at E3 (red) and on the fore reef at E1 (blue). The 24 h, M2 and high-frequency (5–30 min) internal wave band frequencies are plotted in green dashed lines. Panel **b** shows the daily temperature range at different locations and the cumulative net atmospheric heat flux for each day. The shaded area represents 1 SD of the data in the linear fit.

than on the deeper fore reef slope (slope of red line in Fig. 3b is approximately three times larger than blue and green).

There are cold water intrusions evident on the reef flat, which generally occur when currents on the reef flat are directed onshore in the morning. During these intrusions, approximately 2–3°C cooler water from the fore reef is drawn onto the reef flat by tide-, wave-, and wind-driven currents and is transported toward the lagoon. In certain cases (such as on the 08 June), a cold-water intrusion begins, and the cold-water mass is quickly pushed back offshore by changing tidal currents (Fig. 2e).

Reef flat heat budget

A heat budget (Eq. 5) was constructed for the reef flat using near-bed temperature from the DTS and velocity and water depth measurements at E3 and E5 (Supporting Information Fig. S1). Figure 2i shows the heating rate observed on the reef at Mooring E3 and the heating rate predicted from the heat budget estimation for a composite-day average. A simple balance of atmospheric heating and advection of heat across the reef flat was found to adequately predict observed heating rates for a composite day (Fig. 2i; $R^2 = 0.64$, $p < 0.001$). The advective (ΔF) and atmospheric (Q_N) heat flux are similar in magnitude, and both vary substantially on times scales of days. The atmospheric heat flux (Q_N) is dominated by net shortwave (Q_S) and latent (Q_E) heat flux. Solar heating is large on 04–06 June and 09–11 June due to clear skies and smaller on 07–08 June due to clouds. Advective heat flux increases near the end of the deployment due to larger tidal currents and increased wind- and wave-driven flow across the reef.

Over the whole reef flat (Fig. 4), the heat budget reproduces DTS-observed reef-flat temperatures with an average Wilmott Score of 0.91 (Eq. 10), for the 8-d study period. The heat budget for 05 June (Fig. 4b) shows similar patterns to the observed (Fig. 4a) onshore flow of cold water in the morning and solar heating on the reef flat mid-day. From our observations during this deployment, the advection of offshore water onto the reef flat and surface heat flux from solar heating control the variability of temperature on the reef flat. From a simple balance of atmospheric and advective heat flux, given an offshore boundary condition, initial condition across the reef flat, and circulation on the reef, we can predict spatial variability in temperature on the reef flat.

Discussion

Influence of internal waves on reef flat temperatures

For our study period, advective heat flux is important in driving cooling on the reef flat, by bringing offshore water from the fore reef onto the reef flat. In addition to direct observations of the shoreward transport of cold subthermocline waters all the way to the surf zone on Dongsha by internal bores (K. A. Davis unpubl.), internal wave cooling of the fore reef

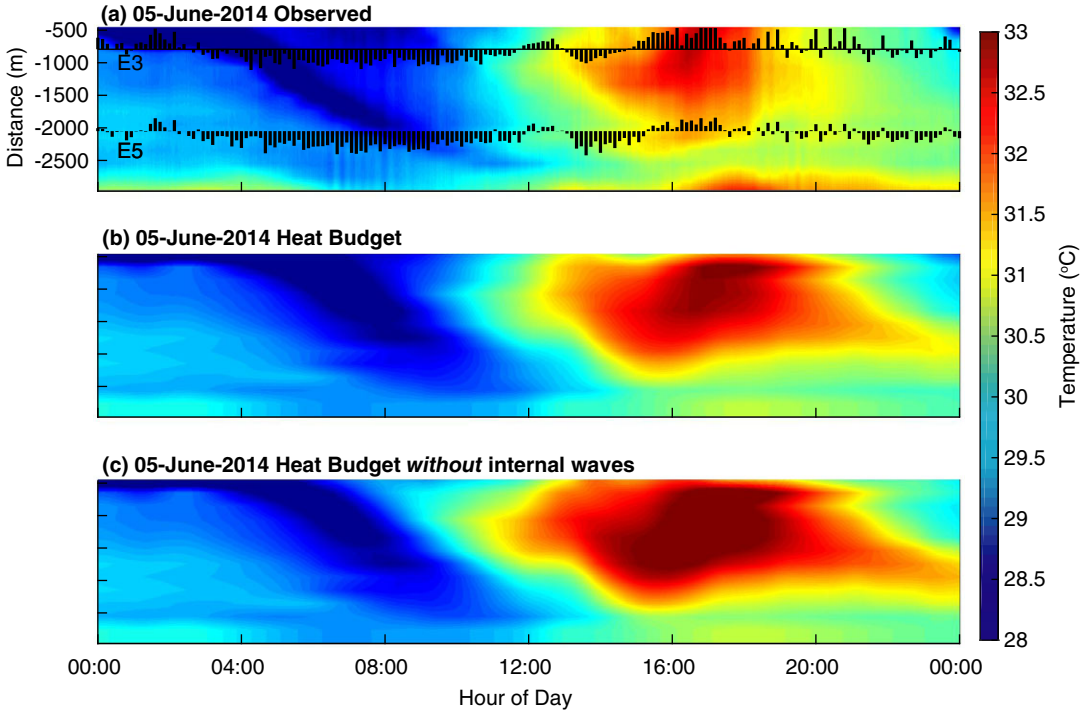

Fig. 4. DTS temperature and heat budget model. Panel **a** shows the observed DTS temperature on the reef for 05 June 2014. The data are averaged in 200 m sections. Across-shore currents are shown at E3 and E5 in black quivers, with quivers pointing down indicating onshore flow (to the west) and quivers pointing up indicating offshore flow (to the east). Panel **b** shows the modeled reef flat temperature using the model described in Heat Budget section. Panel **c** shows the modeled reef flat temperature without internal waves.

water is suggested by an average MODIS SST image for June to August 2002–2017 (Fig. 5a). A cold crescent on the northeast side of the atoll, where internal waves directly impinge, is evident. We averaged MODIS SST in a 3 km^2 area at a location 700 m offshore of the reef crest (Point A; Fig. 5a) and a location approximately 6.5 km offshore of the reef crest (Point B). At the deeper offshore location (Point B), shipboard observations by Fu et al. (2012) have shown that the internal waves are still in coherent form as waves of depression and have not yet forced cool water to the surface as they do further onshore on the shallow slope (Point A). Observations during this experiment near Point A (approximately 50 m depth) indicate that the internal waves are in highly nonlinear form (K. A. Davis unpubl.) and can transport cold subthermocline water shoreward all the way to the reef crest ($\sim$ 1 m depth; e.g., Fig. 2). During summer months (June to August), when internal wave forcing is strongest in the SCS (Ramp et al. 2010), the average difference in SST between Points A and B (ΔSST_{AB}) is 0.22°C $\pm$ 0.01°C, with offshore waters being warmer (Fig. 5a). This difference is smaller during the winter months (ΔSST_{AB} = 0.10°C $\pm$ 0.01°C) when the internal wave field in the SCS is diminished. Further evidence that the cooling on the fore reef is driven by remote internal wave forcing is that ΔSST_{AB} is largest 2 d after the maximum tidal currents in the Luzon Strait (Fig. 5b), which corresponds to the approximate travel time for internal waves between the Luzon Strait and Dongsha Atoll (Ramp et al. 2004; Ramp et al. 2010).

In addition to internal waves, here we discuss other oceanographic processes that could explain the observed cooling on the north-east reef slope. Nineteen years (1992–2010) of REDOS data output (Experiment section) from Zeng et al. (2014) show depth averaged currents during the month of June east of Dongsha Atoll are 10 cm s^{-1} to the south-west, consistent with currents observed at E1 during this study. Southward-directed currents along the east fore reef slope would lead to downwelling, due to Ekman transport, so we do not expect this to be a source of cold water to the east side of Dongsha Atoll during our deployment. The DCE (Site Description section) originates near the south/southwest side of the atoll and travels south/southwest, driving upwelling in the center of the eddy and downwelling on the outside. Due to the location and direction of propagation of the eddy, it does not seem likely to be driving the pattern of observed cooling on the east side of Dongsha. Island wakes can also be a source for upwelled waters (Heywood et al. 1996; Coutis and Middleton 2002; Dong et al. 2007). However, as flow around Dongsha is on average toward the southwest from REDOS output, we would expect a wake to develop on the lee (southwest) side of the atoll (Coutis and Middleton 2002) and this is not consistent with the observed SST pattern. Thus, we conclude that the observed cooling pattern seen on the east fore reef of Dongsha Atoll in the MODIS SST data is primarily due to shoaling large-scale internal waves generated in the Luzon Strait region. Furthermore, we posit that if internal waves were not present, the fore reef water would be

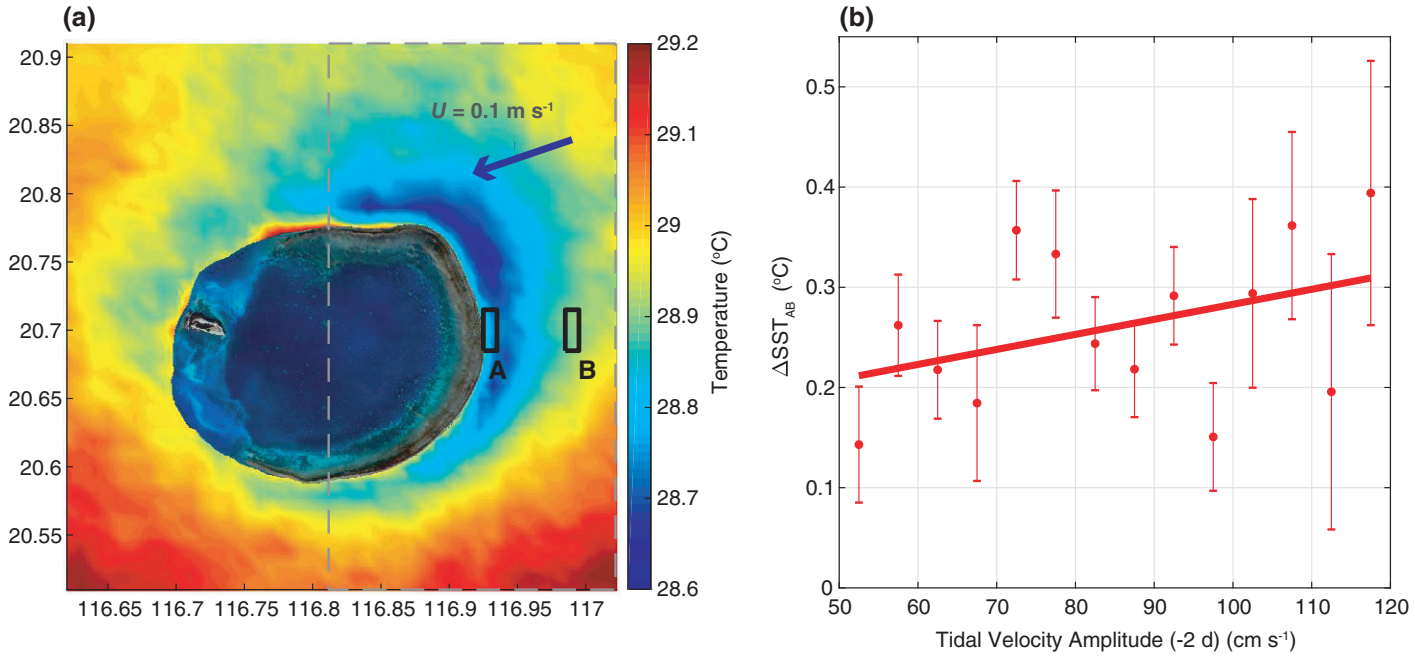

Fig. 5. SST difference and Luzon tidal amplitudes. Panel **a** shows the average MODIS SST data for summer (June to August 2002–2017). The blue arrow shows modeled depth-averaged currents from REDOS within the gray dashed box for summer (June to August 1992–2010) (Zeng et al. 2014). Panel **b** shows the bin averaged SST difference between B and A for summer months (June to August 2002–2017) and the daily range of tidal velocity in the Luzon Strait, 2 d prior to the SST measurements (Egbert and Erofeeva 2002; Padman and Erofeeva 2004).

warmer, and this would make a significant difference in the heat budget on the reef flat.

The important role of advective heat transport in the reef flat heat budget suggests that even though internal waves are not of first-order importance in driving currents on the reef flat, their influence on water properties (e.g., temperature and nutrient concentrations) on the fore reef slope could affect communities on the reef flat when these waters are forced onto the reef flat by local tidal currents and surface gravity waves. In order to estimate the temperature of the fore reef waters without the influence of internal waves, the difference between the temperature on the reef crest and the mean offshore (Point B) SST during our deployment (ΔT_{IW}) was added to the fore reef temperature (boundary condition) in the heat budget (Fig. 4c). The difference between the mean temperature at the reef crest (from the DTS measurements) and the mean offshore SST during our deployment was 0.6°C with offshore SST being higher. Over the 8-d observation period, the composite heat budget suggests that cold subthermocline water delivered to the shallow fore reef by internal waves makes its way onto the reef and contributes to cooling of the reef flat. The location of Point B was chosen because we know the form of the wave there, but we acknowledge that a different offshore point would affect our results. We consider the choice of Point B to be conservative, because it may already be in a region of internal wave influenced cooling (Fig. 5a). If we chose a point further offshore where temperature is warmer, the influence would be greater.

To quantify the impact of internal waves on the reef flat, the estimated temperature from the heat budget with and without internal waves was compared. This simple model suggests that without internal waves, instantaneous predicted temperatures can be as high as 2.0°C ± 0.2°C warmer on the reef flat, and on average 0.1°C ± 0.2°C warmer during the study period. The cooling effect of the internal waves on the reef flat water temperatures may have important consequences for the coral community inhabiting the reef flat. For example, it has been shown that thermal stress accumulates over time, and large positive cumulative temperature anomalies can cause bleaching (Glynn and D'croz 1990).

The cumulative difference in predicted temperatures with and without internal waves (ΔT_{reef}) over a composite day is 0.2°C-d near the reef crest and decreases linearly toward the lagoon (Fig. 6). Although it may be intuitive that the section of the reef near the changed boundary condition sees a bigger effect from internal waves, the influence of the offshore boundary on the reef is highly dependent on the cross-reef flow, which in turn depends on the magnitude and direction of the overall flow across the reef. The only way for ΔT_{reef} to vary with distance across the reef flat in our simple model (neglecting mixing and assuming the effect of water temperature on the surface heat flux is negligible) is for changes in cross-reef current strength and direction to drive spatially variable flushing of reef-flat waters over the course of a day. To test this, we calculated the heat budget for 2 d with very different currents (06 June which had smaller magnitude

currents that were tidally reversing and 11 June when currents were stronger, forced by wind and waves and primarily directed toward the lagoon) but held the atmospheric forcing and ΔT_{IW} the same for both days, set to average conditions. The only difference between these two experimental days was the currents, to test the effect of advection on the spatial variability in internal-wave–driven cooling across the reef flat. It is evident that when currents on the reef flat were tidally forced and smaller magnitude (for example, 06 June; Fig. 6), the spatial gradient in ΔT_{reef} across the reef flat was greater. In this case, the internal waves were not influencing the temperature near the lagoon because the ocean water does not reach the lagoon edge of the reef. When currents were unidirectional onshore and higher magnitude (for example, 11 June; Fig. 6), the gradient in ΔT_{reef} was smaller. Also, with stronger flow across the reef flat due to surface waves, we see an increased influence of internal waves toward the lagoon. These tests illustrate the importance of circulation in driving spatially variable residence times, which determine the influence of the offshore boundary condition (internal waves) across the reef.

Temperatures near the reef crest exceeding the maximum monthly mean (28.9°C for Dongsha Atoll) + 1°C threshold were integrated for 1 week, to estimate the degree heating weeks (DHW) metric, commonly used in coral bleaching predictions. The difference between the DHW with and without internal waves (ΔDHW) is 0.7°C-weeks. A synthesis study of factors influencing coral bleaching (Safaie et al. 2018) predicts that an increase in cumulative thermal anomaly, ΔDHW = 0.7°C-weeks would result in approximately four times the probability of a more severe bleaching event on this reef without the influence of internal waves.

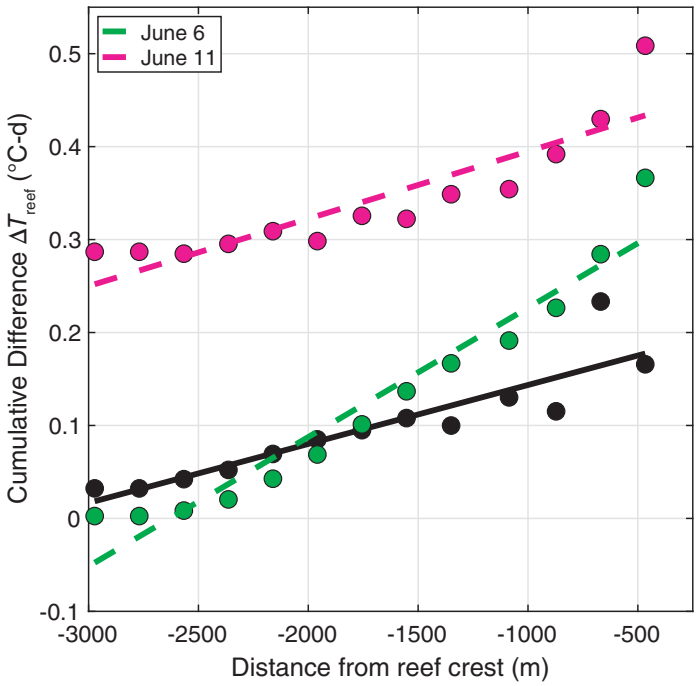

Fig. 6. Cumulative difference without internal waves. The composite daily average of the cumulative difference between the heat budget with internal waves and without internal waves at each location across the reef flat with 0 m representing the reef crest, and −3000 m as the closest location to the lagoon. The black points represent the average for the whole deployment, and the green and pink points represent the test cases where only currents are changed, and other forcing is kept the same.

Cool offshore (on the fore reef) water can provide an important source of cooling for the reef flat, as was seen in June 2015, when low flow on the reef flat, caused by low wind and wave conditions, prevented offshore water from coming onshore (DeCarlo et al. 2017*a*). This led to high residence times and intense heating on the reef flat. Temperatures were 6°C above normal on the reef flat, and widespread bleaching occurred despite no change in internal wave activity in the SCS. This highlights the role of advection on reef flat temperatures, in bringing offshore, internal wave cooled water, and preventing intense heating due to stagnation of water. The increase in probability of a bleaching event, and direct observations of bleaching when internal wave cooled water was not influencing the shallow reef flat, suggest that a reef which experiences internal wave driven cooling may have corals with increased resilience.

Influence of internal waves on reef flat nutrients

Nitrate (NO^{-}_{3}) measurements from water samples taken on the east reef slope and surface waters (< 40 m depth) around Dongsha were used to construct a temperature–nutrient relationship (Fig. 7b). Nitrate concentrations below the detection limit (0.1 μmol L^{-1}) of the sample analysis were not included in the temperature–nutrient relationship. When internal waves shoal on the fore reef slope, cold, high-nutrient water is transported into shallow waters. Shipboard observations on the shallow reef slope (near E1) from 04 June 2014 show when an internal wave arrives, water temperature decreases approximately 4°C and nitrate concentrations 2 m below the surface increase from < 0.1 μmol L^{-1} to approximately 2.0 μmol L^{-1} (Fig. 7a). This high-nutrient water is then available to be transported onto the reef flat by tidal- and wave-driven flow. The temperature–nitrate relationship, DTS temperatures at the reef crest, onshore currents, and depth from E3 were used to estimate nitrate concentration and flux (Fig. 8) at the reef crest. Like the heat budget, ΔT_{IW} was added to the reef crest temperature to estimate the nitrate concentration and flux without internal waves.

In our observations, nitrate flux onto the Dongsha reef flat is episodic in time, peaking when cold water from the fore reef comes onshore past the reef crest. For example, on 07 June 2014 at 23:00:00 h, there is a spike in nitrate flux as offshore water flows onto the reef, but this pulse only lasts for a couple of hours before returning to values below detection level (Fig. 8). Without internal wave influence on the fore reef, we estimate that nitrate fluxes to the reef flat are not significantly above detection level, i.e., are near zero. This is because water coming onto the reef in the no-internal wave case is warmer and has thus lower nitrate concentrations, commonly having

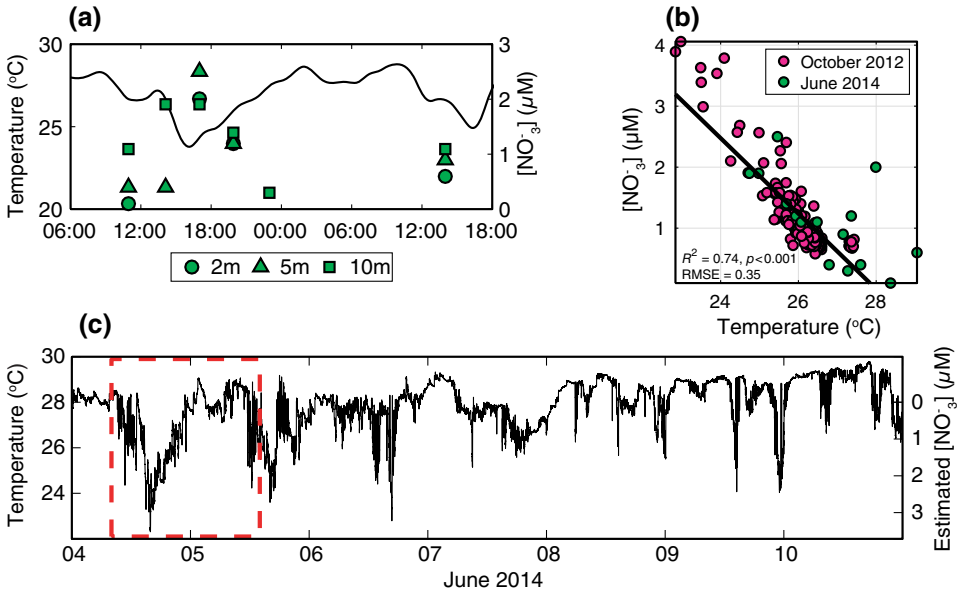

Fig. 7. Temperature–nutrient relationship. Panel **a** shows 3-h low-pass–filtered temperature measurements taken at E1 (depth of 10 m) and nutrient measurements taken at 2, 5, and 10 m depth on 04 and 05 June 2014. Panel **b** shows the temperature–nutrient relationship for measurements taken at locations shown in Fig. 1. Panel **c** shows the temperature at E1 (depth of 10 m) for the whole study period. Nutrient approximations, using the relationship from (**b**), are shown on the right axis.

values of zero when water temperature at the reef crest is above the zero-crossing in the derived temperature–nitrate relationship. If a conservative limit of nitrate minimum concentration (0.1 μmol L^{-1}) is applied, the maximum flux of nitrate onshore through a unit width of the water column was 100.93 $\pm$ 20 μmol s^{-1}, and without internal waves was 21.60 $\pm$ 20 μmol s^{-1}. If we consider a 6-h period on 07 June 2014 when a pulse of offshore water is coming onto the reef (red dashed box; Fig. 8), the cumulative flux of nitrate transported onshore through a unit width of the water column was 5.7 $\pm$ 4.5 $\times$ 10^5 μmol s^{-1}

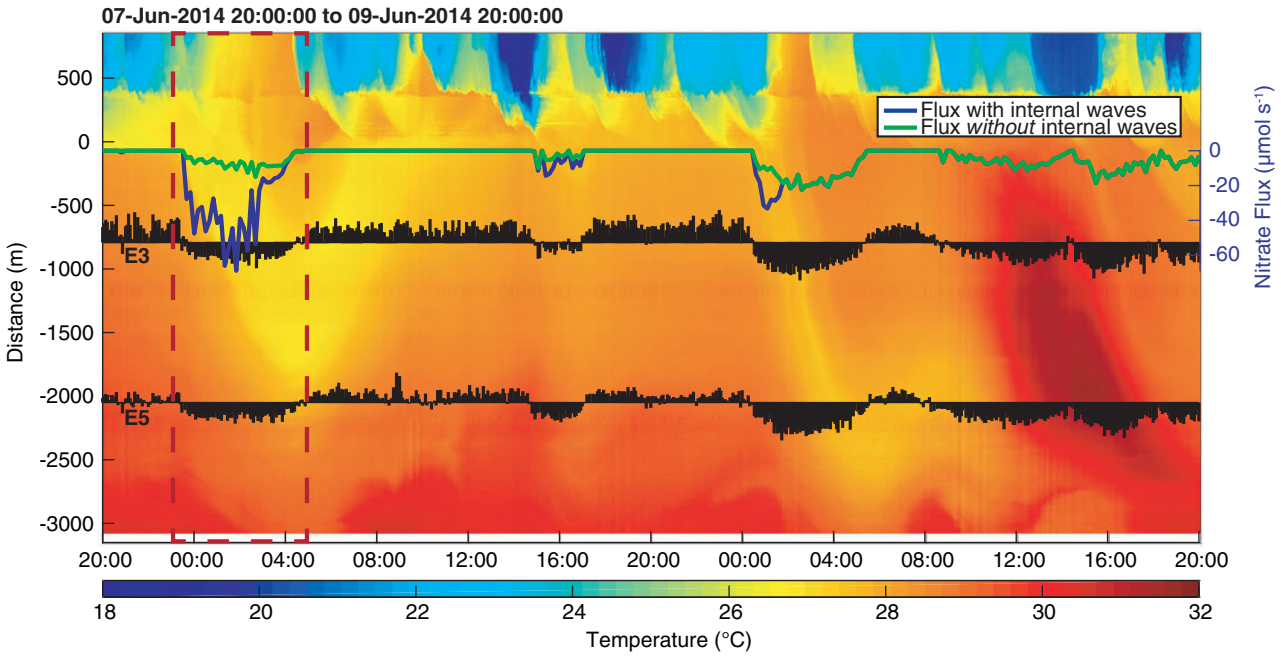

Fig. 8. Nutrient flux. DTS temperature measurements for the 07 June 2014 20:00:00 h to 09 June 2014 20:00:00 h. Across-shore currents are shown at E3 and E5 in black quivers, with quivers pointing in the direction of flow across the reef flat. Onshore nutrient flux with internal waves is shown in blue, just onshore of the reef crest, with negative values indicating an onshore flux of nutrients. Onshore nutrient flux *without* internal waves is shown in green.

with internal waves and $1.3 \pm 4.5 \times 10^5$ μmol s^{-1} without internal waves.

Although the noise in the temperature–nitrate relationship and the detection limit of the nitrate analysis technique introduce uncertainties in the cumulative difference in nitrate fluxes to the reef flat with and without internal waves, our observations suggest that internal waves increase the episodic flux of nitrogen to the reef, and thus play an important role in reef flat productivity. For example, with increased levels of atmospheric CO_2, ocean acidification continues to threaten coral reefs as decreased availability of carbonate ions hinders calcification and skeletal growth (Raven et al. 2005). However, studies have shown that increased heterotrophic feeding or inorganic nutrient availability boosts the energy of corals, which allows them to continue to calcify in low pH seawater (Cohen and Holcomb 2009; Holcomb et al. 2010).

Consequences for reef ecosystems globally

In this study, we show that internal waves can significantly influence the temperature and nutrient environment on the shallow reef flat of Dongsha Atoll and these changes can have implications for the thermal resilience and calcification rates of the reef community. During the 1997–1998 El Niño event, and a 2015 bleaching event, corals on the slopes of Dongsha Atoll that receive internal waves had low mortality, whereas the corals in the lagoon and on the reef flat not exposed to internal wave influence had high mortality rates (Dai 2004; DeCarlo et al. 2017*a*). A study by Tkachenko and Soong (2017) classified the Dongsha fore reef as a thermal refuge for corals, in part due to the influence of internal waves. Internal wave cooled water making its way onto the shallow reef flat has the potential to reduce thermal stress there.

The reef at Dongsha Atoll has higher net ecosystem calcification rates than any other coral reef studied to date, and the internal waves are one of the mechanisms that may contribute to this (DeCarlo et al. 2017*b*). This study showed that net ecosystem production and net ecosystem calcification are tightly linked on the reef flat; therefore, the flux of nutrients onshore due to internal waves could be one of the mechanisms influencing the net ecosystem calcification rates (DeCarlo et al. 2017*b*).

Although Dongsha Atoll is a unique case, due to the large amplitude internal waves that shoal there, internal waves are prominent features throughout the world's oceans, and these temperature and nutrient effects may be common on other coral reefs with internal wave influence. Furthermore, warming of the upper layer of the ocean, due to climate change, has led to an increase in stratification, that is likely accompanied by an increase in internal wave activity in the northern SCS since 1900 (DeCarlo et al. 2015), and this could be occurring in other locations as well.

A literature review documents observations of internal waves in the vicinity of reefs in at least 44 different locations globally, with about half of these being in situ measurements and the other half remote-sensing studies (e.g., Jackson and Apel 2004; Jackson 2007; *see* Supporting Information Table S1 for detailed list of other papers). There have been various studies that have shown the effect of internal waves on coral communities at deeper sites (10 m depth and greater). Wall et al. (2015) showed that in the Andaman Sea, postbleaching mortality of corals was higher in regions unaffected by internal waves compared to internal wave-influenced regions. Furthermore, enhanced growth rates of suspension feeding corals have been observed where internal waves are present (Leichter et al. 1998). Leichter and Genovese (2006) showed that there were higher growth rates of coral in Florida than in Jamaica, due to greater internal wave activity there, and in Florida, they saw 10–40-fold increases in nutrient concentrations with the arrival of internal waves (Leichter et al. 2003). Internal wave influence on shallow reefs is likely more extensive than has been directly observed. Further research may reveal similar conclusions of the effect on the heat budget and nutrient concentrations on shallow coral reefs worldwide. Understanding these impacts can help identify which reefs may be a thermal refuge due to internal wave influence.

Conclusion

The observations and analyses presented here indicate that internal waves arriving at Dongsha Atoll are modifying water properties on the fore reef and significantly affecting the water temperature and nitrate concentrations on a wide, shallow reef flat. Spatially continuous measurements of water temperature across the fore reef and 3-km wide reef flat from the DTS instrument make it possible to connect offshore processes to water properties in nearshore benthic communities and allow for a spatially resolved heat budget.

We find that internal waves shoaling on Dongsha Atoll cool the near-surface waters (SST) on the east fore reef by 0.2°C in summer and that this internal wave influence is both tidally and seasonally modulated (Fig. 5). Internal wave-influenced water on the fore reef is transported onto the shallow reef flat by tides and surface waves and our analysis shows that it can cool the reef by as much as 2.0°C ± 0.2°C, and on average for the deployment by 0.1 ± 0.2°C, and increase instantaneous nitrate fluxes by approximately four-fold. Thus, internal waves generated over 500 km away from Dongsha may play an important role in mediating thermal stress and the metabolism of a very shallow reef ecosystem. For example, estimates from a statistical model of bleaching factors (Safaie et al. 2018) indicate that without internal wave cooling of the Dongsha reef flat, there would be four times the probability of more severe bleaching.

Quantifying the impact of internal waves on the temperature and nutrient budget of a coral reef will help us to understand resilience of corals and why corals thrive in different environments. Internal waves likely play a role in modifying the water properties on other shallow ecosystems, and understanding the magnitude of these impacts is important in a changing climate.

References

Alford, M. H., and others. 2015. The formation and fate of internal waves in the South China Sea. Nature **521**: 65–69. doi:10.1038/nature14399

Barkley, H. C., A. L. Cohen, Y. Golbuu, V. R. Starczak, T. M. DeCarlo, and K. E. Shamberger. 2015. Changes in coral reef communities across a natural gradient in seawater pH. Science Advances **1**: e1500328. doi:10.1126/sciadv.1500328

Barshis, D. J., J. T. Ladner, T. A. Oliver, F. O. Seneca, N. Traylor-Knowles, and S. R. Palumbi. 2013. Genomic basis for coral resilience to climate change. Proc. Natl. Acad. Sci. USA **110**: 1387–1392. doi:10.1073/pnas.1210224110

Budyko, M. I. 1974. Climate and life. 507 Academic Press. ISBN: 9780080954530

Chow, C. H., J. H. Hu, L. R. Centurioni, and P. P. Niiler. 2008. Mesoscale Dongsha cyclonic Eddy in the northern South China Sea by drifter and satellite observations. J. Geophys. Res. Oceans **113**: 1–15. doi:10.1029/2007JC004542

Codiga, D. L. 2011. Unified tidal analysis and prediction using the UTide Matlab functions. Graduate School of Oceanography, University of Rhode Island Narragansett. ftp://www.po.gso.uri.edu/pub/downloads/codiga/pubs/2011Codiga-UTide-Report.pdf

Cohen, A. L., and M. Holcomb. 2009. Why corals care about ocean acidification: Uncovering the mechanism. Oceanography **22**: 118–127. doi:10.5670/oceanog.2009.102

Coutis, P., and J. Middleton. 2002. The physical and biological impact of a small Island wake in the deep ocean. Deep-Sea Res. I Oceanogr. Res. Pap. **49**: 1341–1361. doi:10.1016/S0967-0637(02)00029-8

Dai, C. 2004. Dong-sha Atoll in the South China Sea: Past, present and future. Paper presented at: Islands of the World VIII International Conference, Kinmen Island, Taiwan.

Davis, K. A., S. J. Lentz, J. Pineda, J. T. Farrar, V. R. Starczak, and J. H. Churchill. 2011. Observations of the thermal environment on Red Sea platform reefs: A heat budget analysis. Coral Reefs **30**: 25–36. doi:10.1007/s00338-011-0740-8

DeCarlo, T. M., K. B. Karnauskas, K. A. Davis, and G. T. F. Wong. 2015. Climate modulates internal wave activity in the northern South China Sea. Geophys. Res. Lett. **42**: 831–838. doi:10.1002/2014GL062522

DeCarlo, T. M., A. L. Cohen, G. T. Wong, K. A. Davis, P. Lohmann, and K. Soong. 2017*a*. Mass coral mortality under local amplification of 2 degrees C ocean warming. Sci. Rep. **7**: 44586. https://www.nature.com/articles/srep44586

DeCarlo, T. M., A. L. Cohen, G. T. F. Wong, F.-. K. Shiah, S. J. Lentz, K. A. Davis, K. E. F. Shamberger, and P. Lohmann. 2017*b*. Community production modulates coral reef pH and the sensitivity of ecosystem calcification to ocean acidification. J. Geophys. Res.: Oceans **122**: 745–761. doi:10.1002/2016JC012326

Dong, C., J. C. McWilliams, and A. F. Shchepetkin. 2007. Island wakes in deep water. J. Phys. Oceanogr. **37**: 962–981. doi:10.1175/JPO3047.1

Donner, S. D. 2009. Coping with commitment: Projected thermal stress on coral reefs under different future scenarios. PLoS One **4**: e5712. doi:10.1371/journal.pone.0005712

Egbert, G. D., and S. Y. Erofeeva. 2002. Efficient inverse modeling of barotropic ocean tides. J. Atmos. Ocean. Technol. **19**: 183–204. doi:10.1175/1520-0426(2002)019<0183:EIMOBO>2.0.CO;2

Fabricius, K. E., and others. 2011. Losers and winners in coral reefs acclimatized to elevated carbon dioxide concentrations. Nat. Clim. Chang. **1**: 165–169. doi:10.1038/nclimate1122

Fairall, C. W., E. F. Bradley, D. P. Rogers, J. B. Edson, and G. S. Young. 1996. Bulk parameterization of air-sea fluxes for tropical ocean-global atmosphere coupled-ocean atmosphere response experiment. J. Geophys. Res.: Oceans **101**: 3747–3764. doi:10.1029/95JC03205

Fairall, C. W., E. F. Bradley, J. Hare, A. Grachev, and J. Edson. 2003. Bulk parameterization of air–sea fluxes: Updates and verification for the COARE algorithm. J. Clim. **16**: 571–591. doi:10.1175/1520-0442(2003)016<0571:BPOASF>2.0.CO;2

Fu, K., Y. H. Wang, L. S. Laurent, H. Simmons, and D. P. Wang. 2012. Shoaling of large-amplitude nonlinear internal waves at Dongsha Atoll in the northern South China Sea. Cont. Shelf Res. **37**: 1–7. doi:10.1016/j.csr.2012.01.010

Garrett, C., and W. Munk. 1979. Internal waves in the ocean. Annu. Rev. Fluid Mech. **11**: 339–369. doi:10.1146/annurev.fl.11.010179.002011

Glynn, P. 1993. Coral reef bleaching: Ecological perspectives. Coral Reefs **12**: 1–17. doi:10.1007/BF00303779

Glynn, P., and L. D'croz. 1990. Experimental evidence for high temperature stress as the cause of El Nino-coincident coral mortality. Coral Reefs **8**: 181–191. doi:10.1007/BF00265009

Goreau, T. J., and R. L. Hayes. 1994. Coral bleaching and ocean" hot spots". Ambio-J. Human Environ. Res. Manage. **23**: 176–180. https://www.researchgate.net/profile/Thomas_Goreau/publication/245800342_Coral_Bleaching_and_Ocean_Hot_Spots/links/0a85e53a43e67c75c7000000.pdf

Green, R. H., N. L. Jones, M. D. Rayson, R. J. Lowe, C. E. Bluteau, and G. N. Ivey. 2018. Nutrient fluxes into an isolated coral reef atoll by tidally driven internal bores. Limnol. Oceanogr. 1–3. doi:10.1002/lno.11051. https://aslopubs.onlinelibrary.wiley.com/doi/epdf/10.1002/lno.11051

Hausner, M. B., F. Suarez, K. E. Glander, N. van de Giesen, J. S. Selker, and S. W. Tyler. 2011. Calibrating single-ended fiber-optic Raman spectra distributed temperature sensing data. Sensors (Basel) **11**: 10859–10879. doi:10.3390/s111110859

Heywood, K. J., D. P. Stevens, and G. R. Bigg. 1996. Eddy formation behind the tropical Island of Aldabra. Deep-Sea Res. I Oceanogr. Res. Pap. **43**: 555–578. doi:10.1016/0967-0637(96)00097-0

Hoegh-Guldberg, O. 1999. Climate change, coral bleaching and the future of the world's coral reefs. Mar. Freshw. Res. **50**: 839–866. doi:10.1071/MF99078

Hoegh-Guldberg, O., and others. 2007. Coral reefs under rapid climate change and ocean acidification. Science **318**: 1737–1742. doi:10.1126/science.1152509

Hofmann, G. E., and others. 2011. High-frequency dynamics of ocean pH: A multi-ecosystem comparison. PLoS One **e28983**: 6. doi:10.1371/journal.pone.0028983

Holcomb, M., D. C. McCorkle, and A. L. Cohen. 2010. Long-term effects of nutrient and CO 2 enrichment on the temperate coral *Astrangia poculata* (Ellis and Solander, 1786). J. Exp. Mar. Biol. Ecol. **386**: 27–33. doi:10.1016/j.jembe.2010.02.007

Hsu, M.-K., and A. K. Liu. 2000. Nonlinear internal waves in the South China Sea. Can. J. Remote Sens./J. Can. Teledetect. **26**: 72–81. doi:10.1080/07038992.2000.10874757

Hu, J., H. Kawamura, H. Hong, and Y. Qi. 2000. A review on the currents in the South China Sea: Seasonal circulation, South China Sea warm current and Kuroshio intrusion. J. Oceanogr. **56**: 607–624. doi:10.1023/A:1011117531252

Jackson, C. R., and J. Apel. 2004. An atlas of internal solitary-like waves and their properties. Contract **14**: 0176. http://ww.internalwaveatlas.com/Atlas2_PDF/IWAtlas2_FrontMatter.pdf

Jackson, C. 2007. Internal wave detection using the moderate resolution imaging Spectroradiometer (MODIS). J. Geophys. Res. **112**: 1–13. doi:10.1029/2007JC004220. https://agupubs.onlinelibrary.wiley.com/doi/epdf/10.1029/2007JC004220

Kobs, S., D. M. Holland, V. Zagorodnov, A. Stern, and S. W. Tyler. 2014. Novel monitoring of Antarctic ice shelf basal melting using a fiber-optic distributed temperature sensing mooring. Geophys. Res. Lett. **41**: 6779–6786. doi:10.1002/2014GL061155

Leichter, J. J., and S. J. Genovese. 2006. Intermittent upwelling and subsidized growth of the scleractinian coral Madracis mirabilis on the deep fore-reef slope of Discovery Bay, Jamaica. Marine Ecology Progress Series **316**: 95–103. doi:10.3354/meps316095

Leichter, J. J., S. R. Wing, S. L. Miller, and M. W. Denny. 1996. Pulsed delivery of subthermocline water to conch reef (Florida keys) by internal tidal bores. Limnol. Oceanogr. **41**: 1490–1501. doi:10.4319/lo.1996.41.7.1490

Leichter, J. J., G. Shellenbarger, S. J. Genovese, and S. R. Wing. 1998. Breaking internal waves on a Florida (USA) coral reef: A plankton pump at work? Mar. Ecol. Prog. Ser. **166**: 83–97. doi:10.3354/meps166083

Leichter, J. J., H. L. Stewart, and S. L. Miller. 2003. Episodic nutrient transport to Florida coral reefs. Limnol. Oceanogr. **48**: 1394–1407. doi:10.4319/lo.2003.48.4.1394

Lentz, S. J., J. H. Churchill, K. A. Davis, J. T. Farrar, J. Pineda, and V. Starczak. 2016. The characteristics and dynamics of wave-driven flow across a platform coral reef in the Red Sea. J. Geophys. Res.: Oceans **121**: 1360–1376. doi:10.1002/2015JC011141

Lentz, S. J., K. A. Davis, J. H. Churchill, and T. M. DeCarlo. 2017. Coral reef drag coefficients–water depth dependence. J. Phys. Oceanogr. **47**: 1061–1075. doi:10.1175/JPO-D-16-0248.1

Lucas, A. J., P. J. Franks, and C. L. Dupont. 2011. Horizontal internal-tide fluxes support elevated phytoplankton productivity over the inner continental shelf. Limnol. Oceanogr.: Fluids Environ. **1**: 56–74. doi:10.1215/21573698-1258185

Maritorena, S., A. Morel, and B. Gentili. 1994. Diffuse reflectance of oceanic shallow waters: Influence of water depth and bottom albedo. Limnol. Oceanogr. **39**: 1689–1703. doi:10.4319/lo.1994.39.7.1689

McClanahan, T., J. Maina, R. Moothien-Pillay, and A. Baker. 2005. Effects of geography, taxa, water flow, and temperature variation on coral bleaching intensity in Mauritius. Mar. Ecol. Prog. Ser. **298**: 131–142. doi:10.3354/meps298131

McPhee-Shaw, E. E., D. A. Siegel, L. Washburn, M. A. Brzezinski, J. L. Jones, A. Leydecker, and J. Melack. 2007. Mechanisms for nutrient delivery to the inner shelf: Observations from the Santa Barbara Channel. Limnol. Oceanogr. **52**: 1748–1766. doi:10.4319/lo.2007.52.5.1748

Monsen, N. E., J. E. Cloern, L. V. Lucas, and S. G. Monismith. 2002. A comment on the use of flushing time, residence time, and age as transport time scales. Limnol. Oceanogr. **47**: 1545–1553. doi:10.4319/lo.2002.47.5.1545

Moore, C., J. R. Koseff, and E. L. Hult. 2016. Characteristics of bolus formation and propagation from breaking internal waves on shelf slopes. J. Fluid Mech. **791**: 260–283. doi:10.1017/jfm.2016.58

Morton, B., and G. Blackmore. 2001. South China Sea. Mar. Pollut. Bull. **42**: 1236–1263. doi:10.1016/S0025-326X(01)00240-5

Nash, J. D., E. L. Shroyer, S. M. Kelly, M. E. Inall, T. F. Duda, M. D. Levine, N. L. Jones, and R. C. Musgrave. 2012. Are any coastal internal tides predictable? Oceanography **25**: 80–95. doi:10.5670/oceanog.2012.44

Noble, M., B. Jones, P. Hamilton, J. Xu, G. Robertson, L. Rosenfeld, and J. Largier. 2009. Cross-shelf transport into nearshore waters due to shoaling internal tides in San Pedro Bay, CA. Cont. Shelf Res. **29**: 1768–1785. doi:10.1016/j.csr.2009.04.008

Padman, L., and S. Erofeeva. 2004. A barotropic inverse tidal model for the Arctic Ocean. Geophys. Res. Lett. **31**: 1–4. doi:10.1029/2003GL019003. https://agupubs.onlinelibrary.wiley.com/doi/epdf/10.1029/2003GL019003

Palumbi, S. R., D. J. Barshis, N. Traylor-Knowles, and R. A. Bay. 2014. Mechanisms of reef coral resistance to future climate change. Science **344**: 895–898. doi:10.1126/science.1251336

Pan, X., G. T. F. Wong, T. M. DeCarlo, J.-H. Tai, and A. L. Cohen. 2017. Validation of the remotely sensed nighttime sea surface temperature in the shallow waters at the Dongsha Atoll. Terr. Atmos. Ocean. Sci. **28**: 517–524. doi:10.3319/TAO.2017.03.30.01

Pandolfi, J. M., S. R. Connolly, D. J. Marshall, and A. L. Cohen. 2011. Projecting coral reef futures under global

warming and ocean acidification. Science **333**: 418–422. doi:10.1126/science.1204794

Pineda, J., V. Starczak, A. Tarrant, J. Blythe, K. Davis, T. Farrar, M. Berumen, and J. C. B. da Silva. 2013. Two spatial scales in a bleaching event: Corals from the mildest and the most extreme thermal environments escape mortality. Limnol. Oceanogr. **58**: 1531–1545. doi:10.4319/lo.2013.58.5.1531

Ramp, S. R., Y. Yang, and F. Bahr. 2010. Characterizing the nonlinear internal wave climate in the northeastern South China Sea. Nonlinear Process. Geophys. **17**: 481–498. doi:10.5194/npg-17-481-2010

Ramp, S. R., and others. 2004. Internal solitons in the northeastern South China Sea. Part I: Sources and deep water propagation. IEEE J. Ocean. Eng. **29**: 1157–1181. doi:10.1109/JOE.2004.840839

Raven, J., and others. 2005. Ocean acidification due to increasing atmospheric carbon dioxide. The Royal Society. http://oceanrep.geomar.de/7878/1/965_Raven_2005_OceanAcidificationDueToIncreasing_Monogr_pubid13120.pdf

Reed, R. K. 1976. On estimation of net long-wave radiation from the oceans. J. Geophys. Res. **81**: 5793–5794. doi:10.1029/JC081i033p05793

Riegl, B., and W. E. Piller. 2003. Possible refugia for reefs in times of environmental stress. Int. J. Earth Sci. **92**: 520–531. doi:10.1007/s00531-003-0328-9

Rosenfeld, L. K., F. B. Schwing, N. Garfield, and D. E. Tracy. 1994. Bifurcated flow from an upwelling center: A cold water source for Monterey Bay. Cont. Shelf Res. **14**: 931–964. doi:10.1016/0278-4343(94)90058-2

Safaie, A., and others. 2018. High frequency temperature variability reduces the risk of coral bleaching. Nat. Commun. 9. doi:10.1038/s41467-018-04074-2

Selker, J. S., and others. 2006. Distributed fiber-optic temperature sensing for hydrologic systems. Water Resour. Res. 42. doi:10.1029/2006WR005326

Shamberger, K. E., A. L. Cohen, Y. Golbuu, D. C. McCorkle, S. J. Lentz, and H. C. Barkley. 2014. Diverse coral communities in naturally acidified waters of a Western Pacific reef. Geophys. Res. Lett. **41**: 499–504. doi:10.1002/2013GL058489

Sinnett, G., and F. Feddersen. 2014. The surf zone heat budget: The effect of wave heating. Geophys. Res. Lett. **41**: 7217–7226. doi:10.1002/2014GL061398

Spalding, M. D., and B. E. Brown. 2015. Warm-water coral reefs and climate change. Science **350**: 769–771. doi:10.1126/science.aad0349

Suárez, F., M. B. Hausner, J. Dozier, J. S. Selker, and S. W. Tyler. 2011. Heat transfer in the environment: Development and use of fiber-optic distributed temperature sensing. *In* Dr. Marco Aurelio Dos Santos Bernardes (Ed.), Developments in heat transfer. InTech, 611–636. ISBN: 978-953-307-569-3, Available from: http://www.intechopen.com/books/developments-in-heat-transfer/heat-transfer-in-the-environmentdevelopment-and-use-of-fiber-optic-distributed-temperature-sensing

Tkachenko, K. S., and K. Soong. 2017. Dongsha Atoll: A potential thermal refuge for reef-building corals in the South China Sea. Mar. Environ. Res. **127**: 112–125. doi:10.1016/j.marenvres.2017.04.003

Tyler, S. W., J. S. Selker, M. B. Hausner, C. E. Hatch, T. Torgersen, C. E. Thodal, and S. G. Schladow. 2009. Environmental temperature sensing using Raman spectra DTS fiber-optic methods. Water Resour. Res. **45**: 1–11. doi:10.1029/2008WR007052

Van Emmerik, T., A. Rimmer, Y. Lechinsky, K. Wenker, S. Nussboim, and N. Van de Giesen. 2013. Measuring heat balance residual at lake surface using distributed temperature sensing. Limnol. Oceanogr. Methods **11**: 79–90. doi:10.4319/lom.2013.11.79

Van Hooidonk, R., and others. 2016. Local-scale projections of coral reef futures and implications of the Paris agreement. Sci. Rep. **6**: 39666. https://www.nature.com/articles/srep39666/

van Woesik, R., K. Sakai, A. Ganase, and Y. Loya. 2011. Revisiting the winners and the losers a decade after coral bleaching. Mar. Ecol. Prog. Ser. **434**: 67–76. doi:10.3354/meps09203

van Woesik, R., P. Houk, A. L. Isechal, J. W. Idechong, S. Victor, and Y. Golbuu. 2012. Climate-change refugia in the sheltered bays of Palau: Analogs of future reefs. Ecol. Evol. **2**: 2474–2484. doi:10.1002/ece3.363

Vercauteren, N., H. Huwald, E. Bou-Zeid, J. S. Selker, U. Lemmin, M. B. Parlange, and I. Lunati. 2011. Evolution of superficial lake water temperature profile under diurnal radiative forcing. Water Resour. Res.: **47**: 1–10. doi:10.1029/2011WR010529

Wall, M., L. Putchim, G. M. Schmidt, C. Jantzen, S. Khokiattiwong, and C. Richter. 2015. Large-amplitude internal waves benefit corals during thermal stress. Proc. Biol. Sci. **282**: 20140650. doi:10.1098/rspb.2014.0650

Walter, R. K., C. B. Woodson, R. S. Arthur, O. B. Fringer, and S. G. Monismith. 2012. Nearshore internal bores and turbulent mixing in southern Monterey Bay. J. Geophys. Res. Oceans **117**: 1–13. doi:10.1029/2012JC008115

Walter, R. K., C. B. Woodson, P. R. Leary, and S. G. Monismith. 2014. Connecting wind-driven upwelling and offshore stratification to nearshore internal bores and oxygen variability. J. Geophys. Res.: Oceans **119**: 3517–3534. doi:10.1002/2014JC009998

Wang, Y.-H., C.-F. Dai, and Y.-Y. Chen. 2007. Physical and ecological processes of internal waves on an isolated reef ecosystem in the South China Sea. Geophys. Res. Lett. **34**: 1–7. doi:10.1029/2007GL030658

Willmott, C. J. 1982. Some comments on the evaluation of model performance. Bull. Am. Meteorol. Soc. **63**: 1309–1313. https://journals.ametsoc.org/doi/pdf/10.1175/1520-0477%281982%29063%3C1309%3ASCOTEO%3E2.0.CO%3B2

Wolanski, E., and G. Pickard. 1983. Upwelling by internal tides and Kelvin waves at the continental shelf break on the great barrier reef. Mar. Freshw. Res. **34**: 65–80. doi:10.1071/MF9830065

Wolanski, E., and B. Delesalle. 1995. Upwelling by internal waves, Tahiti, French Polynesia. Cont. Shelf Res. **15**: 357–368. doi:10.1016/0278-4343(93)E0004-R

Wong, G. T. F., T.-L. Ku, H. Liu, and M. Mulholland. 2015*a*. The oceanography of the northern South China Sea Shelf-Sea (NoSoCS) and its adjacent waters—overview and Highlights1. Elsevier.

Wong, G. T. F., X. Pan, K.-Y. Li, F.-K. Shiah, T.-Y. Ho, and X. Guo. 2015*b*. Hydrography and nutrient dynamics in the northern South China Sea shelf-sea (NoSoCS). Deep-Sea Res. II Top. Stud. Oceanogr. **117**: 23–40. doi:10.1016/j.dsr2.2015.04.026

Wong, G. T. F., L. Li-Tzu Hou, and K. Y. Li. 2017. Preservation of seawater samples for soluble reactive phosphate, nitrite, and nitrate plus nitrite analyses by the addition of sodium hydroxide. Limnol. Oceanogr. Methods **15**: 320–327. doi:10.1002/lom3.10160

Woodson, C. 2018. The fate and impact of internal waves in nearshore ecosystems. Annu. Rev. Mar. Sci. **10**: 421–441. doi:10.1146/annurev-marine-121916-063619

Zeeman, M. J., J. S. Selker, and C. K. Thomas. 2014. Near-surface motion in the nocturnal, stable boundary layer observed with fibre-optic distributed temperature sensing. Bound.-Layer Meteorol. **154**: 189–205. doi:10.1007/s10546-014-9972-9

Zeng, X., S. Peng, Z. Li, Y. Qi, and R. Chen. 2014. A reanalysis dataset of the South China Sea. Sci. Data **1**: 140052. doi:10.1038/sdata.2014.52

Zimmerman, R. C., and J. N. Kremer. 1984. Episodic nutrient supply to a kelp forest ecosystem in Southern California. J. Mar. Res. **42**: 591–604. doi:10.1357/002224084788506031

Acknowledgments

We are grateful for the support of the Dongsha Atoll Research Station and the Dongsha Atoll Marine National Park, whose efforts made this research possible. The authors would also like to thank G. Lohmann from Woods Hole Oceanographic Institution and L. Hou, F. Shiah, and K. Lee from Academia Sinica for providing logistical and field support. We thank S. Tyler, and J. Selker from the Center for Transformative Environmental Monitoring Programs, funded by the National Science Foundation (EAR awards 1440596 and 1440506), for timely and effective provision of experimental design support, logistical support, and equipment for the project. We thank R. Branch, University of Washington, and X. Pan, Ocean University of China, for their guidance and SST data that informed this study. Support to G. T. F. Wong is from the Ministry of Science and Technology, Taiwan, grant NSC98-2611-M-001-004-MY3 and NSC100-2611-M-001-001 and from the Academia Sinica through grants titled "Atmospheric Forcing on Ocean Biogeochemistry (AFOBi)" and "Dongsha Ocean Acidification Study (DOcS)". Support for S. Lentz is from National Science Foundation grant OCE-1558343. Support for A. Cohen from NSF Grant No. 1220529, by the Academia Sinica (Taiwan) through a thematic project grant to G. Wong and A. Cohen. Support for E. Reid, A. Safaie, and K. A. Davis is from National Science Foundation grant OCE-1753317, and support to E. Reid from the Environmental Engineering Henry Samueli Endowed Fellowship and the UCI Oceans Graduate Fellowship.

Conflict of Interest

None declared.

Submitted 12 September 2018
Revised 08 February 2019
Accepted 19 February 2019

Associate editor: Craig Stevens